**Scientific Reports**

https://doi.org/10.1038/s41598-026-45381-9

**Article in Press**

# Insights into the antibacterial mode of action of cress polysaccharide-mediated NiO nanoparticles

**Received: 27 January 2026**

**Accepted: 18 March 2026**

Published online: 24 March 2026

**Cite this article as: Jamil Y., Ali M., Ali S. *et al.* Insights into the antibacterial mode of action of cress polysaccharide-mediated NiO nanoparticles. *Sci Rep* (2026). https://doi.org/10.1038/s41598-026-45381-9**

**Yusra Jamil, Mansoor Ali, Sajid Ali, Douglas Law, Abdulwahed Fahad Alrefaei & Ayaz Ahmad**

We are providing an unedited version of this manuscript to give early access to its findings. Before final publication, the manuscript will undergo further editing. Please note there may be errors present which affect the content, and all legal disclaimers apply.

If this paper is publishing under a Transparent Peer Review model then Peer Review reports will publish with the final article.

ARTICLE IN PRESS

© The Author(s) 2026. **Open Access** This article is licensed under a Creative Commons Attribution-NonCommercial-NoDerivatives 4.0 International License, which permits any non-commercial use, sharing, distribution and reproduction in any medium or format, as long as you give appropriate credit to the original author(s) and the source, provide a link to the Creative Commons licence, and indicate if you modified the licensed material. You do not have permission under this licence to share adapted material derived from this article or parts of it. The images or other third party material in this article are included in the article's Creative Commons licence, unless indicated otherwise in a credit line to the material. If material is not included in the article's Creative Commons licence and your intended use is not permitted by statutory regulation or exceeds the permitted use, you will need to obtain permission directly from the copyright holder. To view a copy of this licence, visit http://creativecommons.org/licenses/by-nc-nd/4.0/.

# Insights into the Antibacterial Mode of Action of Cress Polysaccharide-Mediated NiO Nanoparticles

Yusra Jamil[1], Mansoor Ali[1], Sajid Ali[2]*, Douglas Law[3], Abdulwahed Fahad Alrefaei[4], Ayaz Ahmad[1,5]*

[1]Department of Biotechnology, Abdul Wali Khan University Mardan, 23200, Khyber Pakhtunkhwa, Pakistan

[2]Department of Horticulture and Life Science, Yeungnam University, Gyeongsan 38541, Republic of Korea

[3]Faculty of Health and Life Sciences, INTI International University, 71800, Nilai, Negeri Sembilan, Malaysia.

[4]Department of Zoology, College of Science, King Saud University, Riyadh, 11451, Saudi Arabia

[5]Institute of Genetics and Developmental Biology, Chinese Academy of Sciences, Beijing, 100101, China

*Correspondence: ahdayazb5@awkum.edu.pk (A.A.); drsajid@yu.ac.kr (S.A)

## Abstract

The increasing prevalence of antimicrobial resistance necessitates the development of alternative antibacterial strategies. In this study, nickel oxide nanoparticles (NiO NPs) were synthesized using cress (*Lepidium sativum*) seed mucilage polysaccharides (CSP) as a green reducing and stabilizing agent. The formation of CSP-mediated NiO nanoparticles (CSP-NiO) was confirmed through extensive characterization using UV-Visible, FTIR, XRD, SEM, and EDX techniques. The CSP-NiO NPs exhibited minimal erythrocyte toxicity (<5% hemolysis at 200 µg/mL) and dose-dependent antibacterial activity against Gram-positive (*Staphylococcus aureus* and *Clostridium tetani*) and Gram-negative (*Escherichia* coli and *Klebsiella pneumoniae*) bacteria, with MIC values ranging from 25 to 50 µg/mL. The mechanistic investigations revealed increased intracellular reactive oxygen species (ROS) production, membrane disruption (evidenced by protein leakage), and genomic DNA damage in treated bacterial cells. These findings suggest that

CSP-NiO NPs exert antibacterial effects through oxidative stress, leading to membrane disruption and genomic DNA damage, thereby establishing them as a sustainable nanomaterial platform for future antimicrobial applications.

***Keywords*:** Green synthesis, Biocompatibility, Polysaccharides, NiO nanoparticles, Antibiotic resistance, Antibacterial mechanism, ROS, Human health

## 1. Introduction

Antimicrobial resistance (AMR) has emerged as a major challenge in modern healthcare, as resistance to commonly prescribed antibiotics continues to rise worldwide [1, 2]. The growing prevalence of antibiotic-resistant pathogens has intensified research efforts to develop effective and sustainable alternative antimicrobial strategies [3, 4]. In this regard, nanoparticles have attracted significant interest due to their nanoscopic size and high surface-area-volume ratio, which facilitates strong interactions with microbial cell membranes [5, 6]. Metallic nanoparticles, including silver (Ag), nickel (Ni), and cobalt (Co), as well as their oxide derivatives, have demonstrated antibacterial activity against a wide range of pathogenic bacteria [7, 8]. Recent studies have also highlighted the potential of bio-derived nanocomposite materials and metal oxide-based hybrid systems for advanced functional applications, including energy storage and catalytic processes [9]. Nickel oxide nanoparticles (NiO NPs) have received increasing attention over recent years due to their excellent physicochemical stability, catalytic properties, and reported antibacterial potential [10]. Compared with other metal-oxide nanoparticles, NiO NPs offer advantages such as low production cost, environmental compatibility, and a wide optical bandgap of 3.6-4.0 eV [11]. These properties have broadened their applications in antimicrobial research [12, 13]. Experimental findings indicate that NiO NPs exert antibacterial effects through mechanisms including $Ni^{2+}$ ion release, electrostatic interactions with bacterial membranes, oxidative stress induction, and subsequent cellular damage [14-16].

Although various physical and chemical synthesis methods have been widely employed, green synthesis methods are preferred for their operational simplicity, sustainability, and reduced environmental impact [17]. Green approaches use naturally derived reducing and stabilizing agents, including plant extracts and polysaccharides, thereby minimizing the use of toxic chemical reagents [18, 19]. In this context, polysaccharides are particularly suitable biogenic matrices due to their biocompatibility, biodegradability, and abundance of hydroxyl and carboxyl functional groups, which can reduce metal ions and stabilize nanoparticles [20-22].

*Lepidium sativum* (cress) is a natural source of polysaccharides that has garnered attention due to its biochemical profile and wide therapeutic potential [23, 24]. When soaked in water, *L. sativum* seeds release a mucilaginous gel composed predominantly (~90%) of non-starch polysaccharides and (~10%) starch. The high polysaccharide content and abundance of hydroxyl functional groups make cress seed mucilage a suitable candidate for metal ion reduction and nanoparticle stabilization in a green synthesis approach. Previous studies have reported that polysaccharides isolated from cress seed mucilage exhibit a range of biological activities, including antibacterial, antihypertensive, antioxidant, hypoglycemic, and hypolipidemic [25-27], further supporting their relevance as a bioactive matrix for nanoparticle synthesis.

In the present study, purified cress *(L. sativum)* seed mucilage polysaccharides were employed as a biopolymeric template for the green synthesis of CSP-NiO NPs. In contrast to crude plant extract-mediated synthesis, mucilage-derived polysaccharides constitute a hydroxyl-enriched matrix that can modulate nanoparticle stabilization and nano-bio interface interactions. Although reactive oxygen species (ROS) generation, membrane disruption, and metal ion release have been reported as antibacterial mechanisms of NiO NPs, the relative contribution of these pathways under polysaccharide-mediated synthesis conditions remains uncharacterized.

Accordingly, this study aimed to synthesize and characterize CSP-NiO NPs, evaluate their antibacterial activity, and systematically investigate oxidative stress-mediated membrane disruption and genomic damage to clarify the mechanistic basis of their antibacterial action.

## 2. Materials and Methods

### 2.1. Materials and Reagents

Cress seeds were obtained from a local market in Mardan, Pakistan, and confirmed by the Department of Botany at Abdul Wali Khan University, Mardan, Pakistan. Nickel precursor, nitrate hexahydrate ($Ni(NO_3)_2.6H_2O$), Nutrient agar/broth, 2′,7′- Dichlorohydrofluorescein diacetate (DCFH-DA), Triton X-100, bovine serum albumin (BSA), Bradford reagent, hydrogen peroxide ($H_2O_2$), ciprofloxacin, chloramphenicol, and other analytical grade reagents were purchased from recognized commercial suppliers. All the solutions were prepared using distilled water as a solvent.

### 2.2. Isolation and Purification of Polysaccharides

Cress seed mucilage was isolated according to the procedure previously outlined [28, 29], with some adjustments. Twenty grams of seeds were immersed in 1 L of sterile water for 24 h at room temperature with continuous agitation using a magnetic stirrer. The mucilage was collected by filtration through a muslin cloth. The polysaccharides from the mucilage were precipitated using 75% ethanol and purified by centrifugation (5000 rpm, 20 minutes). The precipitated polysaccharides were then dried using a rotary evaporator, weighed, and stored at -20 °C for further use.

### 2.3. Green synthesis of Nickel oxide Nanoparticles (CSP-NiO NPs)

The green synthesis of nickel oxide nanoparticles (CSP-NiO NPs) was achieved using cress seed mucilage polysaccharides (CSP) as a natural reducing and stabilizing agent. Figure 1 depicts the eco-friendly synthesis process of CSP-NiO NPs using cress seed mucilage polysaccharides. One gram (1 g) of precipitated cress mucilage polysaccharides was dissolved in 50 mL of deionized water and heated to 60 °C. Then, 50 mL of nickel nitrate hexahydrate ($Ni(NO_3)_2.6H_2O$) solution (0.1 mM) was added dropwise to the polysaccharide solution under continuous stirring for 2 hours. The formation of a grayish-black colloidal mixture indicated the synthesis of CSP-NiO NPs. The mixture was centrifuged at 12000 rpm for 15 minutes to collect the precipitate. The pellet was subsequently resuspended in deionized water and washed two to three times to eliminate residual impurities. Afterward, the pellet was dried and calcinated at 300 °C for 2 hours. The synthesis parameters were selected in accordance with the previously reported green NiO NPs protocol [30]. The resultant nanoparticles were ground into a fine blackish-gray powder using a mortar and pestle and stored in an airtight vial for further characterization.

**Figure 1**. Flowchart representing the green synthesis of NiO nanoparticles using Cress mucilage polysaccharides.

## 2.4. Characterization of CSP-NiO NPs

The physicochemical and morphological characteristics of the green-synthesized CSP-NiO NPs were determined using the application of UV–Visible spectroscopy (UV-Vis), Fourier Transform Infrared Spectroscopy (FT-IR), X-ray Diffraction (XRD), Scanning Electron Microscopy (SEM), and Energy Dispersive X-ray Spectroscopy (EDX).

### 2.4.1 UV–Visible Spectroscopic (UV-Vis) Analysis

The bio-reduction of $Ni^{+2}$ ions and the successful formation of CSP-NiO nanoparticles were initially verified by an observable color change from light green to blackish-grey. The UV-visible absorption spectra of green-synthesized CSP-NiO NPs were recorded in the 200-800 nm range using a

UV-visible spectrophotometer (Shimadzu UV-1800, Japan), with distilled water used as the blank reference.

### 2.4.2 Fourier Transform Infrared (FT-IR) Spectroscopic Analysis

Fourier transform infrared (FTIR) spectroscopy was employed to identify the functional groups associated with CSP-NiO NPs. The FTIR spectra were recorded using an FTIR spectrophotometer (Nicolet 870) within the range of 400–4000 $cm^{-1}$ using the KBr pellet method. The resulting absorption bands obtained were attributed to the corresponding functional groups and nickel-oxygen stretching vibrations.

### 2.4.3 X-ray Diffraction (XRD) Analysis

The XRD patterns were recorded using an X-ray diffractometer (Model D8, Germany) to determine the crystalline structure and phase purity of CSP-NiO NPs. The diffraction pattern was obtained over a 2θ range of 10—80° using Cu Kα radiation (λ = 1.54 Å), conducted under controlled conditions. The resulting diffractogram was utilized to ascertain the crystalline phase and lattice planes. The crystallite size and lattice strain were evaluated using the Williamson-Hall (W-H) equation as follows:

$$\beta\cos\theta = \frac{k\lambda}{D} + 4\epsilon\sin\theta$$

Where $\beta$ represents the full width at half-maximum (FWHM) of the diffraction peak, $\theta$ refers to the Bragg angle, $K$ is the shape factor (0.9), $\lambda$ denotes the wavelength of the X-ray radiation employed for diffraction (λ = 1.54 Å), $D$ is the crystalline nanoparticle size, and $\theta$ represents the lattice strain [31].

### 2.4.4. Scanning Electron Microscopy (SEM) and Energy Dispersive X-ray Spectroscopy (EDX) Analyses

SEM was used to characterize the size and shape of the green-synthesized CSP-NiO NPs. The nanoparticle powder was mounted on conductive carbon tape (Nisshin model 731) and coated with a thin gold layer via sputter coating (Cressington, Model 108A). SEM imaging was performed using a Tuscan MIRA3 LMU microscope at 20 kV. The elemental composition of the nanoparticles was assessed by EDX in the 0–10 keV range using the same microscope employed for SEM imaging.

### 2.5. Hemolysis Assay

The hemolytic assay was conducted to evaluate the biocompatibility of CSP and CSP-NiO NPs against human red blood cells (HRBCs). A 5 mL of freshly collected blood from a healthy human donor was centrifuged at 1500 rpm for 15 minutes to obtain the red blood cell (RBC) pellet. The collection and use of human blood was approved by the Institutional Ethics Committee of the Department of Biotechnology, AWKUM, in compliance with the declaration of Helsinki (Ethical Approval Certificate: AWKUM/Biotech/2024/170). All procedures were performed in accordance with relevant ethical guidelines and regulations, and informed consent was obtained from healthy volunteers before blood collection. The pellet was washed several times with autoclaved normal saline (pH 7.4) and resuspended in autoclaved phosphate-buffered saline (PBS) at a 1:3 proportion. Different concentrations of CSP and CSP-NiO NPs were added individually to 100 µL of the RBCs suspension and incubated at 37 ºC for 1 h. After incubation, the samples were centrifuged at 3000 rpm for 10 minutes. The spectrophotometric readings were taken at 570 nm after 100 µL of the aqueous phase was transferred into a micro-well plate. Triton X-100 (0.5%) and phosphate-buffered saline (PBS) were used as positive and negative controls.

The percentage of hemolysis was calculated using the following formula:

$$\text{Hemolysis (\%)} = \frac{(\text{Mean OD of Sample - Mean OD of PBS})}{(\text{Mean OD of Positive control - Mean OD of PBS})} * 100$$

### 2.6. Bacterial Strains and Culture Conditions Used for Antibacterial Activity

The antibacterial activity of CSP and CSP-NiO nanoparticles was tested against four clinically isolated pathogenic bacteria, including Gram-positive (*Clostridium tetani* and *Staphylococcus aureus*) and Gram-negative (*Klebsiella pneumoniae* and *Escherichia coli*). These isolates were obtained from the Pathology Department of Mardan Medical Complex, Pakistan, and cultured on nutrient agar. Each bacterial strain was aseptically inoculated into 5mL of nutrient broth and incubated at 37 °C with continuous agitation to achieve a cell density of approximately $1 \times 10^5$ colony-forming units per milliliter (CFU/mL) equivalent to a 0.5 McFarland standard.

### 2.7. Agar Well Diffusion Assay

The agar well diffusion method was used to determine the antibacterial activity of CSP and CSP-NiO nanoparticles, as reported in a previous study [32]. In brief, bacterial cultures incubated for 24 hours were spread uniformly on nutrient agar plates using sterile cotton swabs. Wells of 6 mm diameter were aseptically punched into the agar through an autoclaved well borer. Varying concentrations of CSP and CSP-NiO NPs (200, 100, and 50 µg/mL) were loaded into the wells and incubated under optimal growth conditions (37 °C for 24 h). Ciprofloxacin discs were used as a positive control for comparative zone-of-inhibition analysis, while sterile distilled water served as a negative control solvent. After incubation, the antibacterial activity was evaluated by measuring the inhibition zone diameter (in millimeters) formed around the wells.

### 2.8. Determination of Minimum Inhibitory and Bactericidal Concentration (MIC and MBC)

The MIC and MBC of CSP and CSP-NiO NPs were determined following the previously reported method [33]. A 100 µL aliquot of CSP and CSP-NiO NPs in serially decreasing concentrations (200-1 µg/mL) was loaded into each well of a 96-well microplate having 100 µL of nutrient broth. Serial dilutions were prepared using a two-fold dilution method, and 100 µL of bacterial inoculum was loaded into the corresponding wells. Nutrient broth without bacterial inoculation served as a sterility control, while sterile distilled water (used as a dispersion solvent) served as a negative control. Chloramphenicol was used as a positive control for MIC determination as it is a standard broad-spectrum antibiotic commonly employed in broth microdilution assays. The microplate was incubated under optimal conditions (37 °C for 24 hours), and optical turbidity at 600 nm was measured using a BioTek Microplate Spectrophotometer (USA) before and after incubation to validate the MIC values. The MIC endpoint was defined as the lowest concentration of each tested sample at which no noticeable bacterial growth was observed. The MBC was established by transferring 2 µL inoculum from wells with no visible growth onto nutrient agar plates and incubating at 37 °C for 24 hours.

### 2.9. Bacterial Growth Kinetics

Bacterial growth was measured using a 96-well microplate. The wells were inoculated with nutrient broth containing a bacterial inoculum of $1 \times 10^5$ CFU/mL and exposed to CSP and CSP-NiO NPs at concentrations of 50, 100, and 200 µg/mL. Optimal conditions were maintained by incubating the microplate at 37 °C with constant agitation at 130 rpm. OD 600 was measured at 5-hour intervals for up to 25 hours of incubation [34].

### 2.10. Quantification of Reactive Oxygen Species (ROS)

Reactive oxygen species (ROS) generated in bacterial cells were measured using the 2′,7′-dichlorohydrofluorescein diacetate (DCFH-DA) assay [35], a commonly used fluorescent indicator of intracellular oxidative stress. Bacterial cell suspensions were standardized to $1 \times 10^5$ CFU/mL and incubated with varying concentrations (50, 100, and 200 µg/mL) of CSP and CSP-NiO NPs at 37 °C for 6 hours under constant agitation. After incubation, the cultures were treated with DCFH-DA (200 □M) and incubated in the dark for 1 hour. Cells treated with 1 mM hydrogen peroxide ($H_2O_2$) were the positive control for ROS generation, while untreated cells were the negative control. The fluorescence intensity of dichlorohydrofluorescein (DCFH), indicative of intercellular ROS production, was measured at an excitation wavelength of 485 nm and an emission wavelength of 535nm. ROS levels were expressed as a percentage relative to the untreated control group.

$$\%\mathrm{ROS} = \frac{\text{Sample Fluorescence}}{\text{Control Fluorescence}} \times 100$$

### 2.11. Protein Leakage Assay

The Bradford assay was used to determine the protein leakage from bacterial cells. Bacterial suspensions (1 × $10^5$ CFU/mL) were treated with different concentrations (50, 100, and 200 µg/mL) of CSP and CSP-NiO NPs and incubated at 37 °C for 6 hours. After the incubation phase, the cultures were centrifuged at 3000 rpm for 10 minutes. Subsequently, 100 µL of each supernatant was mixed with 400 µL of the Bradford reagent and incubated in the dark at 37 °C for 15 minutes. The cells treated with 0.1% Triton X-100 served as the positive membrane disruption control, whereas the untreated bacterial inoculum in broth served as the negative control. The absorbance was recorded at 600 nm, and protein concentration was determined using a bovine serum albumin (BSA) standard curve [36].

### 2.12. DNA Damage Assay

A DNA fragmentation assay was performed to determine the genotoxic effects of CSP and CSP-NiO NPs on bacterial cells [37]. The cultures were exposed to varying concentrations (50, 100, and 200 µg/mL) of the test samples for 24 hours. Genomic DNA was isolated from each sample using the phenol-chloroform-isoamyl alcohol method. The purified DNA was then combined with 5 µL loading dye (bromophenol blue) and loaded onto a 2% agarose gel containing 0.5 µg/mL ethidium bromide. Bacterial DNA samples were resolved by gel electrophoresis at 70 V for 3 h, and the resulting bands were visualized under UV light using the Bio-Rad Gel Doc System.

### 2.13. Statistical Analysis

All quantitative data were expressed as mean ± standard deviation (SD), and experiments were performed in triplicate (n=3). R statistical software was used to perform the statistical analysis. The comparison among different treatment groups was analyzed using one-way ANOVA followed by Tukey’s post hoc test. For the growth kinetics experiment, a two-way ANOVA was used to assess the effects of treatment concentration and incubation time on bacterial growth, with $p < 0.05$ considered statistically significant.

## 3. RESULTS

### 3.1. Green Synthesis of NiO Nanoparticles Using Cress Seeds Polysaccharides

The synthesis of nickel oxide nanoparticles (CSP-NiO NPs) was successfully achieved using polysaccharides extracted from cress *(Lepidium sativum)* seeds mucilage as stabilizers and reducing agents. The interaction between the polysaccharides and the $Ni(NO_3)_2$ salt, carried out for 2 h, resulted in a clear color change to blackish-gray, providing visual evidence of the formation of CSP-NiO NPs. This eco-friendly method highlights the potential of natural biopolymers for the green synthesis of functional nanomaterials.

### 3.2. UV-Visible Spectral Characterization of CSP-NiO NPs

After synthesis, the optical absorption properties of CSP-NiO NPs were analyzed using UV-Visible spectrophotometry in the spectral range 200-800 nm, as shown in Figure 2. The absorption spectrum exhibited a distinct peak at approximately 350 nm, a characteristic of green-synthesized NiO NPs.

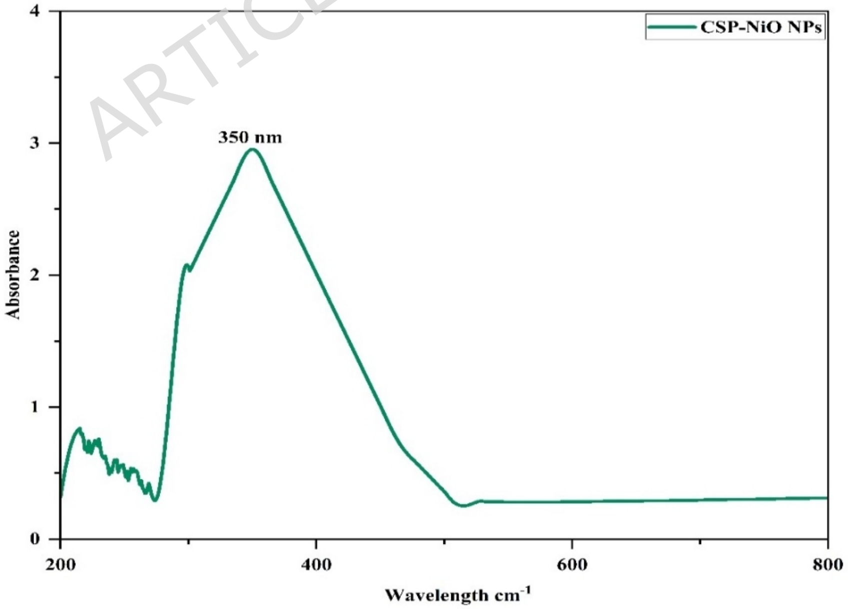

**Figure 2**. The ultraviolet (UV) absorption spectrum of CSP-NiO NPs.

### 3.3 FTIR Spectral Characterization of CSP-NiO NPs

Fourier-transform infrared (FTIR) spectra of CSP-NiO NPs displayed several adsorption bands associated with the surface functional groups and the metal oxygen vibrations, as shown in Figure 3. The broad absorption band near 3324 cm$^{-1}$ is associated with the stretching vibrations of hydrogen-bonded -OH groups, supporting the presence of surface hydroxyls and residual polysaccharide-based components of the green synthesis. The absorption band observed near 1635 cm$^{-1}$ was attributed to bending vibrations associated with surface-bound organic residues. The distinct band observed at 570 cm$^{-1}$ corresponds to Ni-O stretching vibrations, thereby confirming the formation of CSP-NiO NPs. Collectively, the FTIR spectrum corroborates the formation of CSP-NiO NPs and confirms the presence of surface-associated functional groups acquired during the polysaccharide-mediated stabilization.

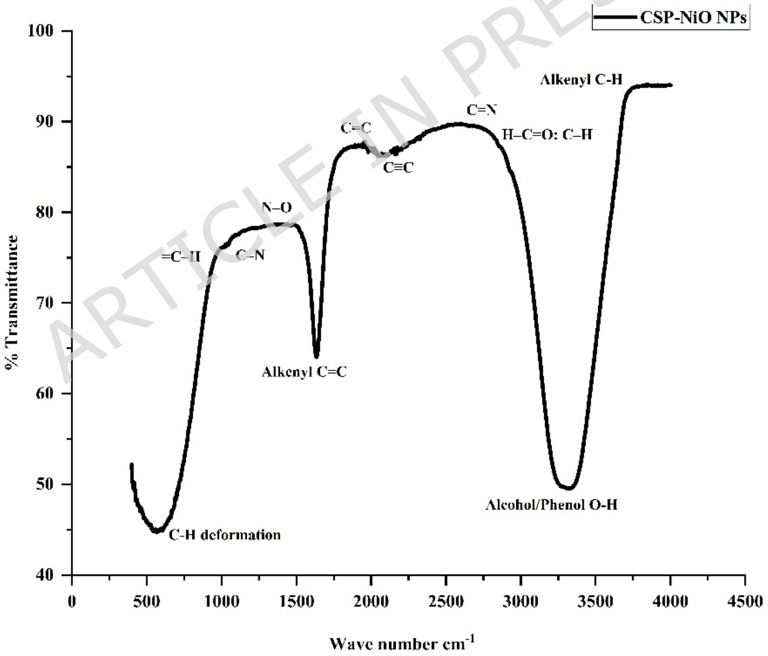

**Figure 3.** FTIR spectroscopic analysis of CSP-NiO NPs.

### 3.4. Crystalline Structure of the CSP-NiO NPs

The crystalline structure of CSP-NiO NPs was confirmed by X-ray diffraction (XRD) analysis. The diffractogram (Figure 4) showed distinct diffraction peaks at 2θ values of approximately 37.4°, 44.1°, 51.3°, 60.9°, and 77.0°.

These peaks correspond to the reported (111), (200), (202), (220), and (311) crystallographic planes of the cubic NiO phase, respectively, confirming the successful formation of crystalline CSP-NiO NPs. The average crystallite size of the synthesized CSP-NiO NPs was analyzed based on the main peaks of the diffraction by using the Williamson-Hall method, yielding an average crystallite size of approximately 16.57 nm with a corresponding lattice strain of ~0.29%. It should be noted that the crystallite size estimated from XRD represents coherently diffracting domains and may not be similar to the larger aggregated structures observed under microscopic observations.

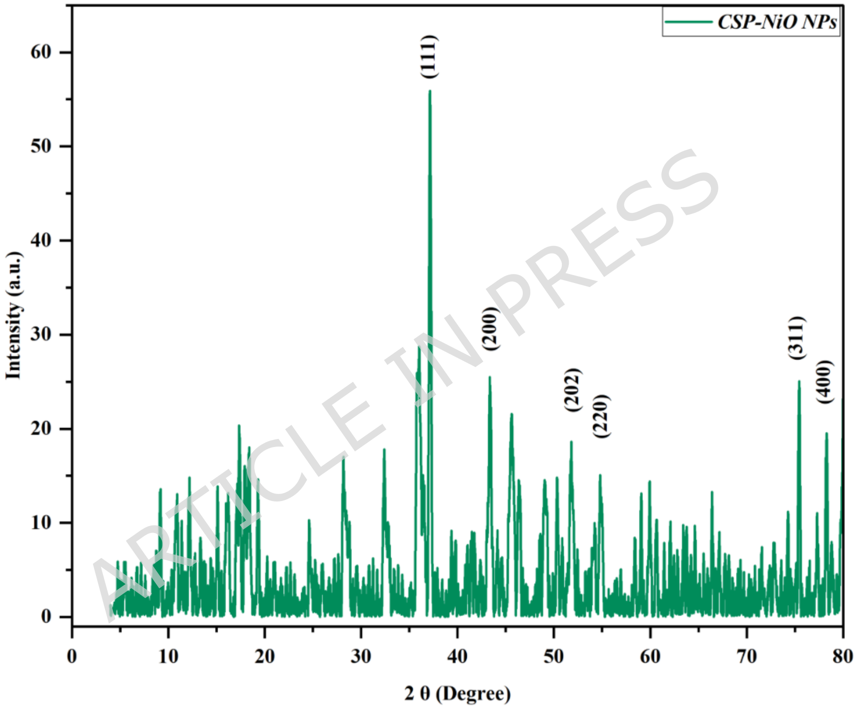

**Figure 4.** XRD pattern of CSP-NiO NPs.

### 3.5. Surface Morphology and Elemental Composition of the CSP-NiO NPs

The surface morphology of CSP-NiO NPs was observed by scanning electron microscopy (SEM) at various magnifications (Figure 5a-g). SEM micrographs indicated that the synthesized material consists of irregularly shaped, agglomerated nanoparticle clusters with rough surface features. At lower magnification, the nanoparticles appear as small micron-scale aggregates, but higher-resolution images reveal that these aggregates contain smaller nanoscale components. Agglomeration is commonly observed in metal-oxide nanoparticles synthesized via green routes, which can result from strong interparticle interactions, surface hydroxylation, and the deposition of polysaccharide-derived surface residues.

The elemental composition of the CSP-NiO NPs was analyzed using energy-dispersive X-ray spectroscopy (EDX). The EDX spectrum indicated the presence of nickel (Ni) and oxygen (O) as the predominant inorganic elements, corroborating the synthesis of NiO NPs (Figure 6). Moreover, signals associated with carbon (C) were detected, likely arising from polysaccharide-derived surface residues or from the carbon tape used during the SEM investigation. Minor trace elements, including Na, S, K, Cl, and Si, were also detected and are likely associated with residual precursor salts, or sample preparation, rather than indicating a distinct crystalline impurity phase.

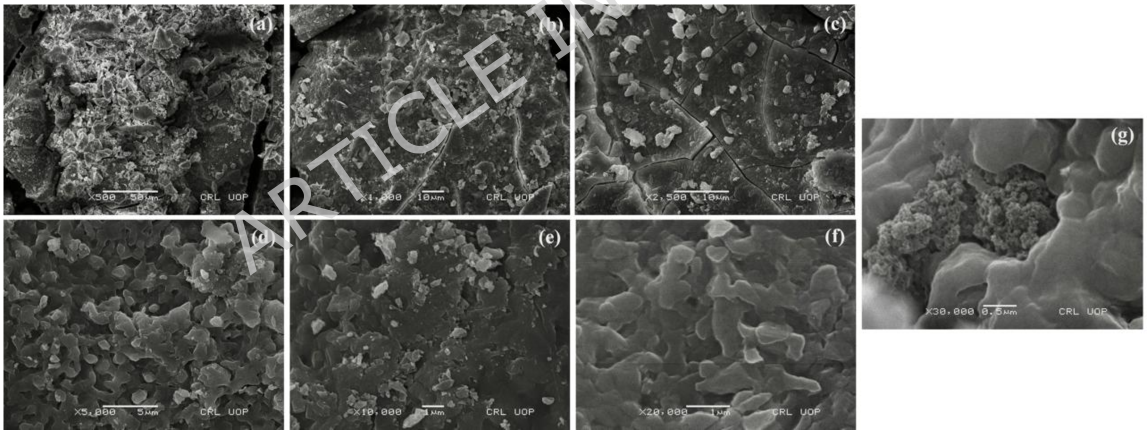

**Figure 5.** SEM micrographs of CSP-NiO NPs recorded at increasing magnifications. (a) ×500, (b) ×1,000 (c) ×2,500 (d) ×5,000 (e) ×10,000 (f) ×20,000 (g) ×30,000.

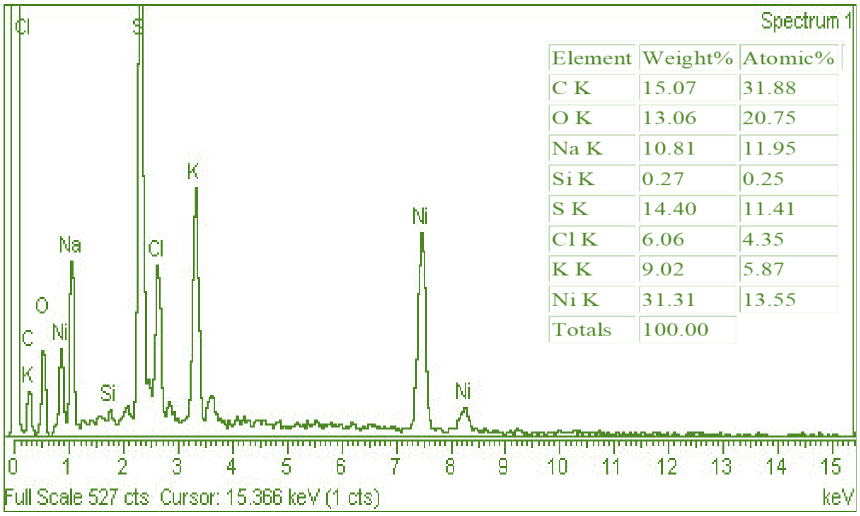

| Element | Weight% | Atomic% |
|---|---|---|
| C K | 15.07 | 31.88 |
| O K | 13.06 | 20.75 |
| Na K | 10.81 | 11.95 |
| Si K | 0.27 | 0.25 |
| S K | 14.40 | 11.41 |
| Cl K | 6.06 | 4.35 |
| K K | 9.02 | 5.87 |
| Ni K | 31.31 | 13.55 |
| Totals | 100.00 | |

**Figure 6.** Elemental composition of CSP-NiO NPs using EDX.

### 3.6. Biocompatibility of the CSP-NiO NPs

The hemolytic activity of CSP and CSP-NiO NPs was determined against freshly obtained normal human erythrocytes. The cytotoxicity was examined at different concentrations and expressed as ± percent hemolysis. No significant hemolysis was observed for CSP and CSP-NiO NPs at all the screening concentrations, as summarized in Figure 7. The results showed that CSP exhibited 0.17 ± 0.32% hemolysis at 25 µg/mL, which increased to 1.90 ± 0.29 % at 200 µg/mL, with a 50% cytotoxic concentration ($CC_{50}$) greater than 10,000 µg/mL. This indicates its compatibility as a stabilizing agent in nanoparticle synthesis. In contrast, the CSP-NiO NPs showed percent hemolysis, ranging from 1.12 ± 0.31% at 25 µg/mL to 5.02 ± 0.89% at 200 µg/mL. The $CC_{50}$ value for CSP-NiO NPs against human erythrocytes was 2,861.22 c. These findings indicate that CSP-NiO NPs exhibit preliminary in vitro hemocompatibility under the tested conditions.

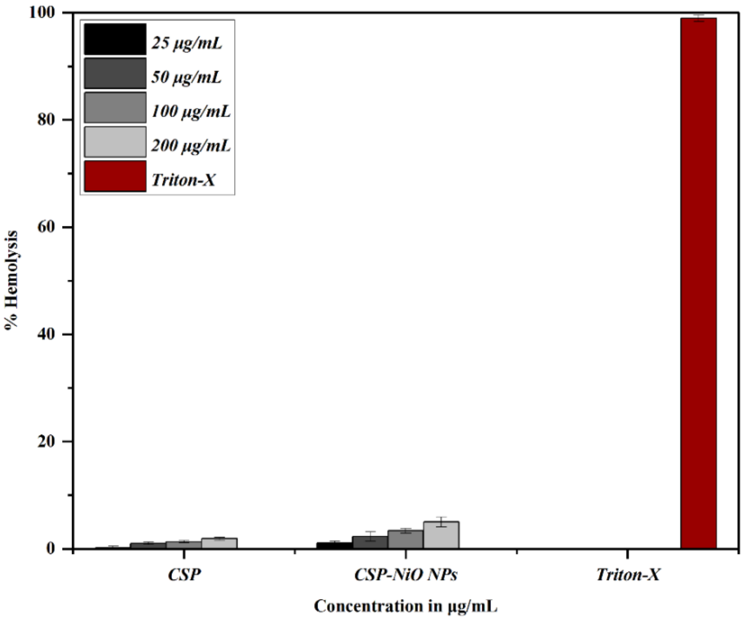

**Figure 7.** Percent hemolysis against human red blood cells (HRBCs) by CSP and CSP-NiO NPs at various screening concentrations (25-200 µg/mL) with Triton-X (0.5%) served as a positive control.

### 3.7 Antibacterial Activity of CSP-NiO NPs Against Clinically Isolated Pathogenic Strains

The antibacterial activity of CSP and CSP-NiO NPs was evaluated against selected pathogenic Gram-positive and Gram-negative bacterial strains using the agar well diffusion method (Figure 8)**.** Both CSP and CSP-NiO NPs displayed dose-dependent antibacterial activity, with an increased zone of inhibition observed as the dose increased from 50 to 200 µg/mL.

For *S. aureus,* CSP produced inhibition zones of 1.25 ± 0.09 mm, 3.25 ± 0.88 mm, and 5.75 ± 1.93 mm at 50, 100, and 200 µg/mL, while CSP-NiO NPs displayed enhanced activity with inhibition zones of 2.50 ± 0.66 mm, 5.50 ± 0.50 mm, and 9.00 ± 0.58 mm at the same concentrations. Similarly, against *C. tetani,* CSP-NiO NPs displayed inhibition zones of 3.75 ± 0.52 mm, 5.25 ± 0.34 mm, and 10.25 ± 0.76 mm at 50, 100, and 200 µg/mL, respectively, representing the maximum observed inhibition. In Gram-negative bacteria, CSP showed no detectable inhibition at 50 µg/mL towards *E. coli* and *K. pneumoniae*; however, measurable inhibition was observed at higher concentrations. CSP-NiO NPs demonstrated enhanced antibacterial activity against *E. coli,* exhibiting inhibition zones of 2.50 ± 0.38 mm, 4.25 ± 0.53 mm, and 10.25 ± 0.58 mm at the same concentrations, with the minimum inhibition recorded at 50 µg/mL. Against *K. pneumoniae*, inhibition zones of 3.75 ± 0.27 mm, 5.75 ± 0.77 mm, and 8.00 ± 0.50 mm were observed at corresponding concentrations. Ciprofloxacin, used as a reference control, exhibited larger inhibition zones (21.9 ± 1.1-24.2 ± 1.0 mm), consistent with its established antibacterial efficacy. Overall, the results demonstrated that CSP-NiO NPs exhibited a moderate dose-dependent antibacterial effect and consistently outperformed CSP alone, particularly against Gram-positive bacteria.

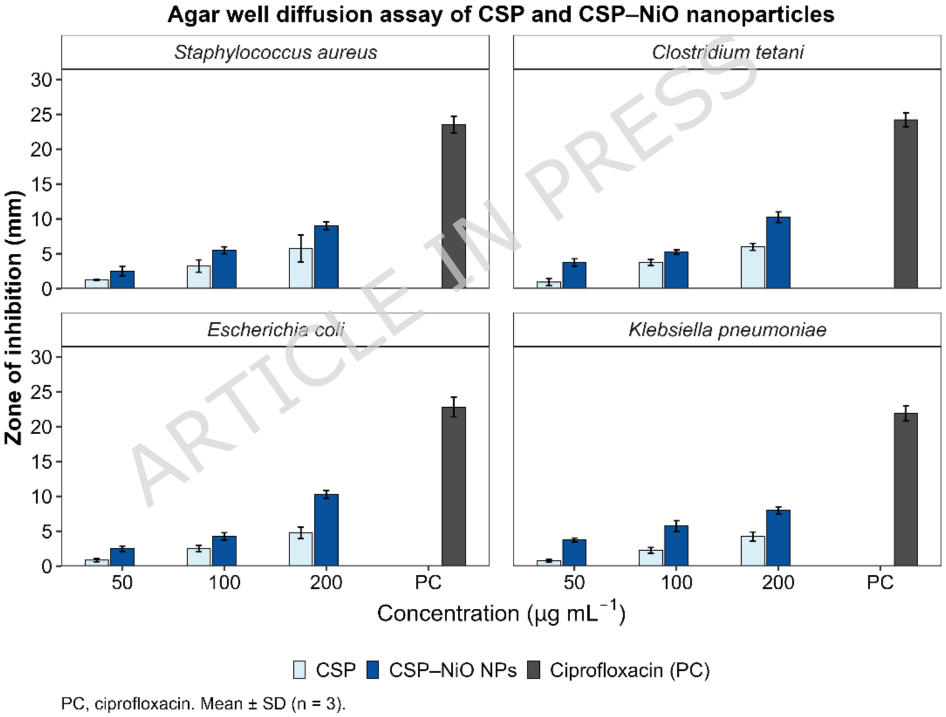

**Figure 8.** Agar well diffusion assay showing the antibacterial activity of CSP and CSP-NiO NPs against *S. aureus, C. tetani, E. coli*, and *K. pneumoniae*. Zone of inhibition was measured at 50, 100, 200 µg/mL$^{-1}$. Ciprofloxacin (PC) served as a positive control. Data are presented as mean ± SD (n = 3).

### 3.8 Minimum Inhibitory Concentration (MIC) and Minimum Bactericidal Concentration (MBC) of CSP-NiO NPs Against Clinically Isolated Pathogenic Strains

The minimum inhibitory concentration (MIC) of CSP and CSP-NiO NPs was evaluated to identify the lowest concentration required to inhibit bacterial growth. The antibacterial effect of CSP, CSP-NiO NPs, and the reference antibiotic chloramphenicol in terms of MIC and MBC is displayed in Table 1. CSP-NiO NPs enhanced antibacterial activity as compared to CSP alone. For Gram-positive bacteria (*S. aureus* and *C. tetani)*, the MIC of CSP-NiO NPs was 25 µg/mL, whereas the corresponding MBC was 50 µg/mL. CSP alone showed relatively higher inhibitory and bactericidal concentrations, with MICs of 50 µg/mL and MBCs of 100 µg /mL against the same bacterial strains. Against Gram-negative bacteria (*E. coli and K. pneumoniae*), CSP-NiO NPs exhibited MIC values of 50 µg /mL and bactericidal activity at 100 µg/mL. CSP required higher concentrations to achieve both an inhibitory and bactericidal effect, as demonstrated by MIC and MBC values of 100 µg/mL against the tested Gram-negative strains. Chloramphenicol, a reference control, showed lower MIC and MBC values than those of the bacterial isolates, as expected for a reference antibiotic. Gram-negative strains exhibited lower sensitivity to CSP-NiO NPs as compared to Gram-positive strains, as evidenced by reduced MIC and MBC levels.

**Table 1.** Minimum inhibitory concentration (MIC) and minimum bactericidal concentration (MBC) of CSP, CSP-NiO NPs, and chloramphenicol against clinically isolated pathogenic strains. Values are expressed as mean ± SD (n = 3), and concentrations are reported in µg/mL.

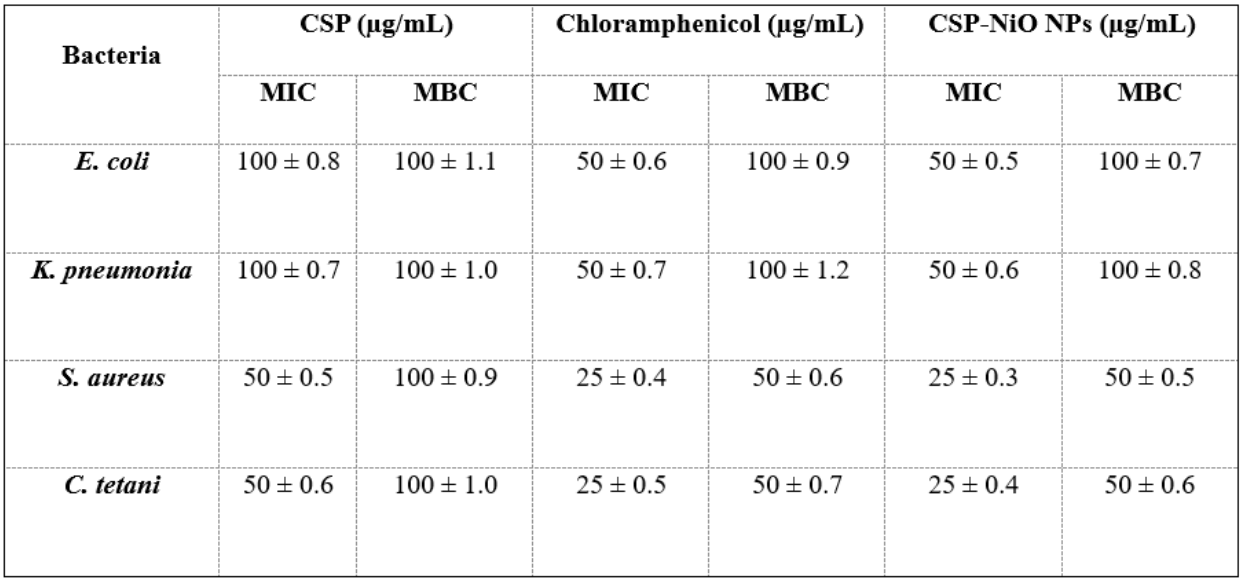

| Bacteria | CSP (µg/mL) | | Chloramphenicol (µg/mL) | | CSP-NiO NPs (µg/mL) | |
|---|---|---|---|---|---|---|
| | MIC | MBC | MIC | MBC | MIC | MBC |
| ***E. coli*** | 100 ± 0.8 | 100 ± 1.1 | 50 ± 0.6 | 100 ± 0.9 | 50 ± 0.5 | 100 ± 0.7 |
| ***K. pneumonia*** | 100 ± 0.7 | 100 ± 1.0 | 50 ± 0.7 | 100 ± 1.2 | 50 ± 0.6 | 100 ± 0.8 |
| ***S. aureus*** | 50 ± 0.5 | 100 ± 0.9 | 25 ± 0.4 | 50 ± 0.6 | 25 ± 0.3 | 50 ± 0.5 |
| ***C. tetani*** | 50 ± 0.6 | 100 ± 1.0 | 25 ± 0.5 | 50 ± 0.7 | 25 ± 0.4 | 50 ± 0.6 |

### 3.9 Growth Kinetics of Bacterial Cells Treated with Different Concentrations of CSP and CSP-NiO NPs

The effects of CSP and CSP-NiO NPs on bacterial proliferation were further illustrated by the bacterial growth curves shown in Figure 9a-b. Untreated control cultures exhibited normal growth, reaching the stationary stage in about 25 hours. Figure 9a shows that CSP treatment reduces bacterial growth, with the reduction increasing with concentration, although growth was not completely inhibited. In contrast, Figure 9b shows that CSP-NiO NPs showed a stronger concentration-dependent bacterial growth inhibition. Growth was partially inhibited at 50 µg/mL. In contrast, at 100 and 200 µg/mL, it was significantly inhibited in Gram-positive (*S. aureus and C. tetani*) and Gram-negative (*E. coli and K. pneumoniae*) species. Overall, Gram-positive strains were more susceptible than Gram-negative strains, with the strongest growth inhibition observed at 200 µg/mL CSP-NiO NPs.

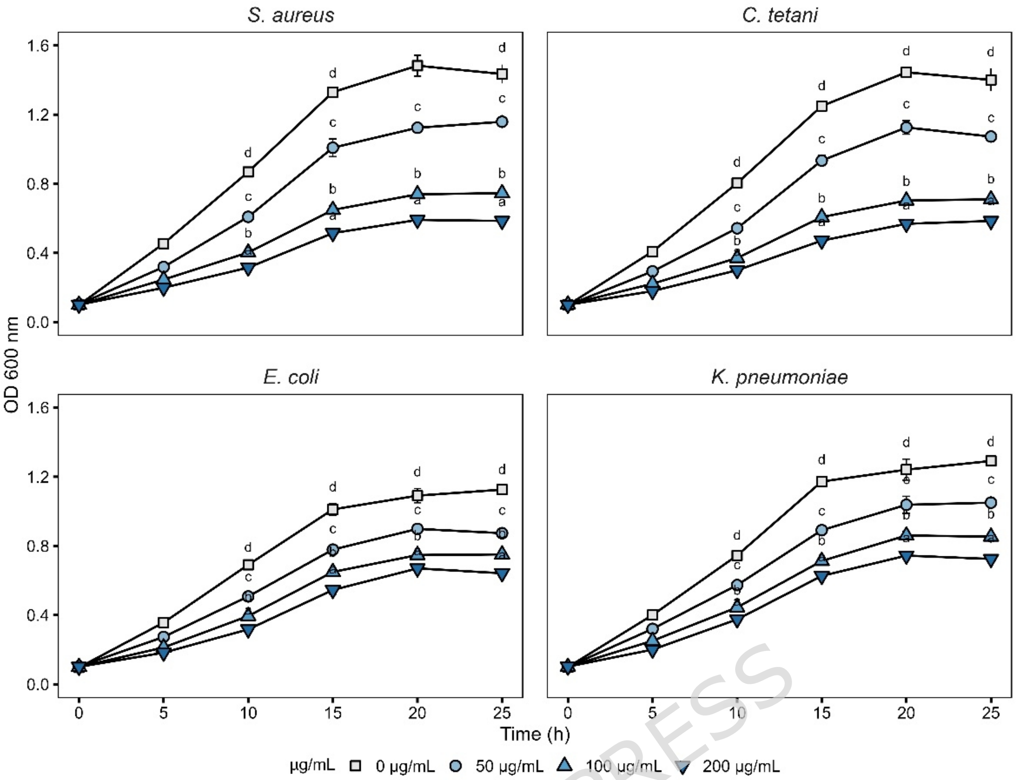

**Figure 9a.** Representative growth kinetic profiles of *S. aureus, C. tetani, E. coli*, and *K. pneumoniae* following exposure to CSP at different concentrations (0-200 µg/mL). Untreated cells (0 µg/mL) served as a control. Optical density at 600 nm (OD600) was recorded at the indicated time intervals over 25 hours. Data represent mean ± SD (n=3). Different letters indicate significant differences among concentrations ($p < 0.05$).

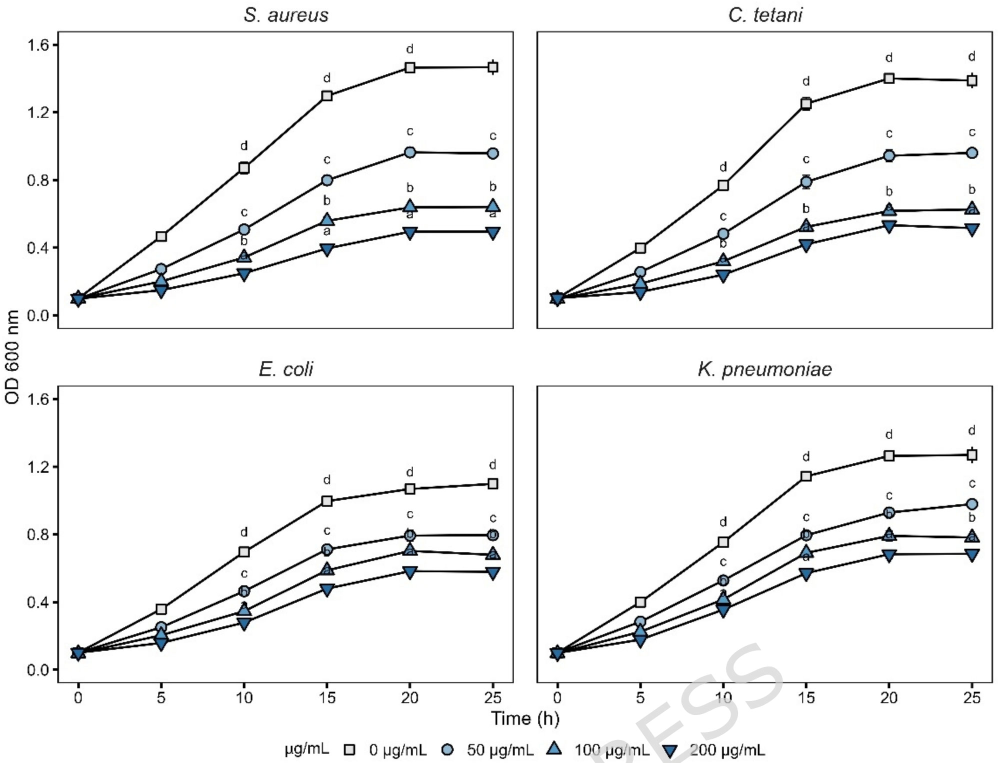

**Figure 9b.** Representative growth kinetic profiles of *S. aureus, C. tetani, E. coli*, and *K. pneumoniae* following treatment with CSP-NiO NPs at different concentrations (0-200 µg/mL). Untreated cells (0 µg/mL) served as a control. Optical density at 600 nm (OD600) was recorded at the indicated time intervals over 25 hours. Data represent mean ± SD (n=3). Different letters indicate significant differences among concentrations ($p < 0.05$).

### 3.10 CSP-NiO NPs Induced Reactive Oxygen Species (ROS) Generation

Intracellular reactive oxygen species (ROS) generation in the bacterial strains treated with CSP and CSP-NiO NPs was quantified using the DCFH-DA fluorescence assay and expressed as a percentage relative to the untreated control. As shown in Figure 10a, CSP treatment resulted in a moderate, concentration-dependent increase in ROS levels, with approximately 1.2-1.4-fold elevation compared to the untreated control. In contrast, Figure 10b shows that CSP-NiO NPs led to a significantly higher elevation in ROS generation across all tested strains. At higher concentrations (100-200 µg/mL), CSP-NiO NPs increased ROS levels by approximately 1.6 to 2.0-fold relative to the control. Among all the tested strains, *S. aureus* exhibited the highest ROS induction, followed by *C. tetani*, whereas *E. coli* and *K. pneumoniae* showed comparatively lower ROS generation. The results indicate that CSP-NiO NPs exert antibacterial activity via oxidative stress.

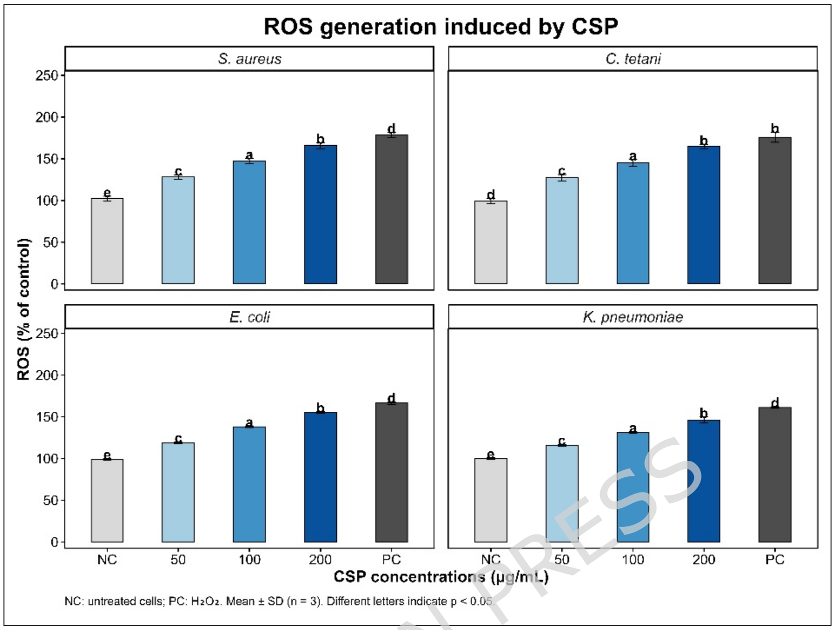

NC: untreated cells; PC: $H_2O_2$. Mean ± SD (n = 3). Different letters indicate $p < 0.05$.

**Figure 10a**. Intracellular ROS generation in bacterial strains treated with CSP at different concentrations (50-200 µg/mL), measured using the DCFH-DA assay and expressed relative to the untreated control.

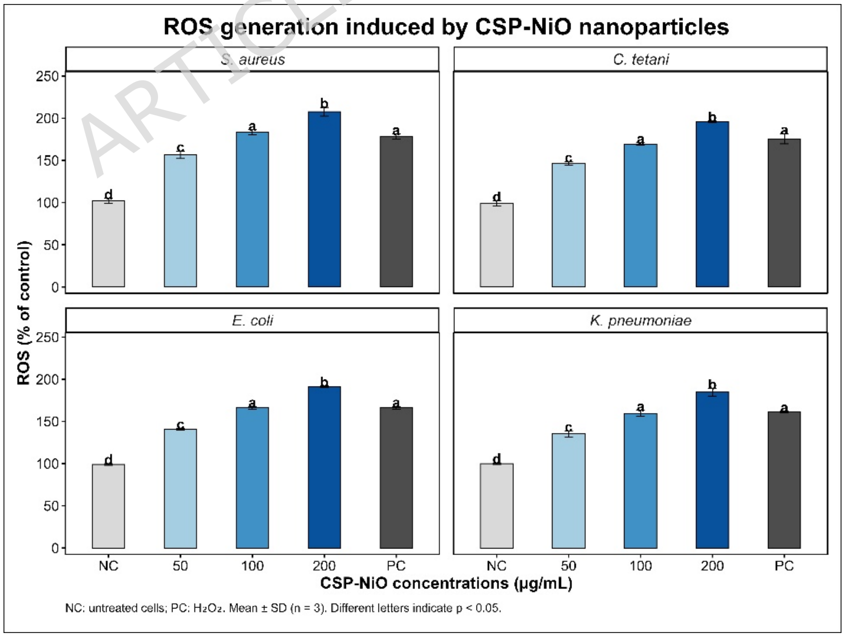

NC: untreated cells; PC: $H_2O_2$. Mean ± SD (n = 3). Different letters indicate $p < 0.05$.

**Figure 10b**. Intracellular ROS generation in bacterial strains treated with CSP-NiO NPs at different concentrations (50-200 µg/mL), measured using the DCFH-DA assay and expressed relative to the untreated control.

## 3.11 Effect of CSP-NiO NPs on Protein Leakage from Bacterial Cell Membranes

The effect of CSP and CSP-NiO NPs on bacterial cell membrane integrity was evaluated by measuring protein leakage (Figure 11a-b). The untreated control cells showed negligible protein release, indicating that the bacterial membranes remained intact under normal growth conditions. Triton-X induced a marked protein efflux, indicating complete disruption of the membrane. As shown in Figure 11a, CSP treatment had a moderate increase in the leakage of proteins, which increased in a concentration-dependent manner but was still lower than the leakage in nanoparticle-treated cells. On the other hand, Figure 11b shows that CSP-NiO NPs cause a strong, concentration-dependent increase in protein leakage in all bacterial strains tested during a 6-hour incubation. Protein efflux increased with increasing nanoparticle concentration and peaked at the highest concentration. In cells treated with CSP-NiO NPs, protein leakage ranged from 18.96 to 38.27 µg/mL in *S. aureus*, 24.51 to 46.23 µg/mL in *C. tetani*, 15.61 to 36.61 µg/mL in *E. coli*, and 14.94 to 27.02 µg/mL in *K. pneumoniae.*

In general, Gram-positive bacteria (*S. aureus and C. tetani*) exhibited higher levels of protein leakage than Gram-negative bacteria, indicating greater membrane vulnerability in CSP-NiO NPs. The elevated protein leakage observed after exposure to CSP-NiO NPs indicated a severe disturbance of bacterial cell membrane integrity.

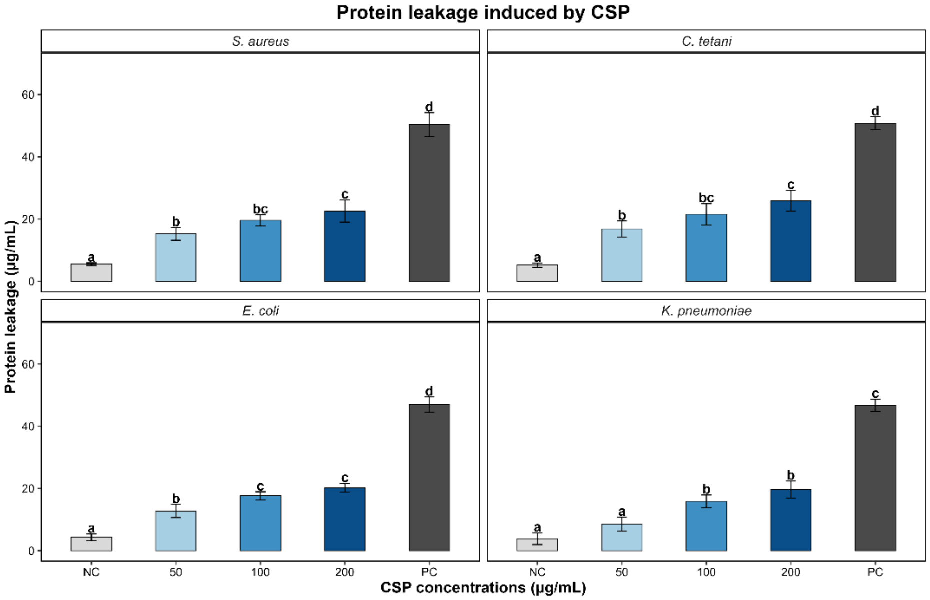

NC: untreated cells in broth. PC: 0.1% Triton X-100. Mean ± SD (n = 3). Different letters indicate Tukey groups ($p < 0.05$).

**Figure 11a.** Protein leakage in pathogenic bacterial strains induced by CSP at different concentrations (50-200 µg/mL) after 6-hour exposure.

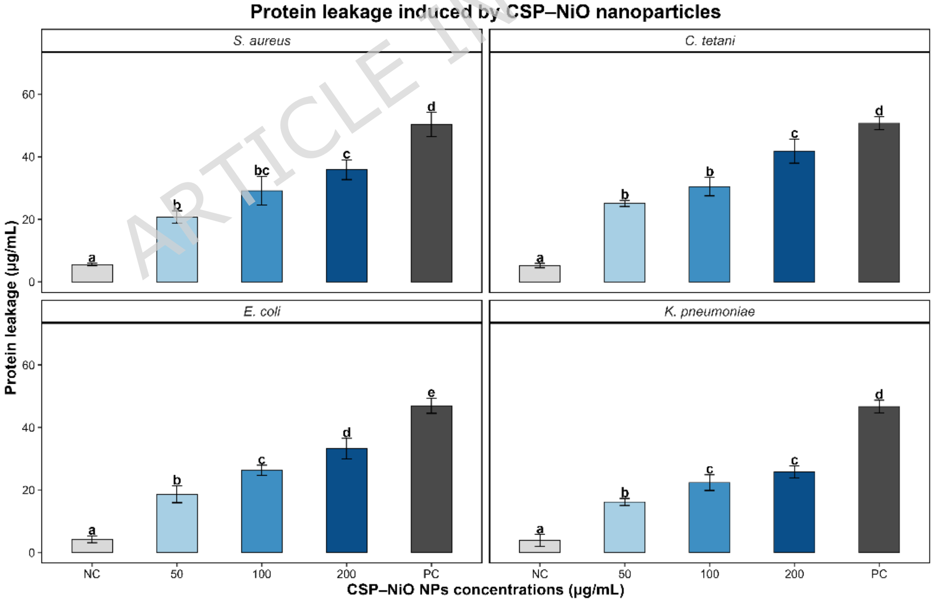

NC: untreated cells in broth. PC: 0.1% Triton X-100. Mean ± SD (n = 3). Different letters indicate Tukey groups ($p < 0.05$).

**Figure 11b.** Protein leakage in pathogenic bacterial strains induced by CSP-NiO NPs at different concentrations (50-200 µg/mL) after 6-hour exposure.

## 3.12 Effect of CSP-NiO NPs on Genomic DNA Integrity

The integrity of bacterial genomic DNA following treatment with CSP and CSP-NiO NPs was assessed using agarose gel electrophoresis (Figure 12). The negative control (untreated cells) showed an intact DNA band without smearing, indicating no loss of genomic integrity. CSP-treated DNA displayed a gradual decrease in band intensity with increasing concentration, accompanied by mild smearing, suggesting concentration-dependent DNA damage.

Conversely, DNA exposed to CSP-NiO-treated cells showed weak bands with extensive smearing, particularly at high concentrations, indicating the disruption of genomic DNA integrity. Overall, CSP-NiO NPs induced more pronounced DNA fragmentation than CSP, indicating greater genotoxicity under the tested conditions.

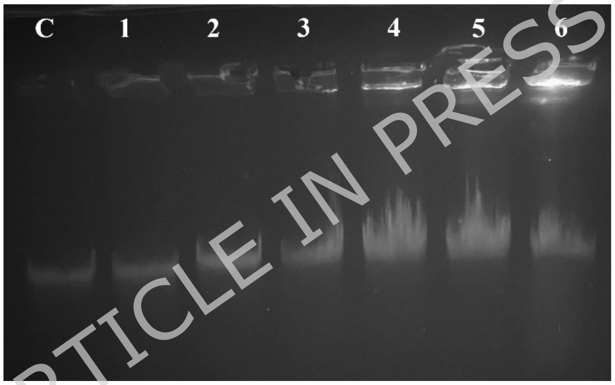

**Figure 12.** Bacterial DNA fragmentation by CSP and CSP-NiO NPs. Lane C: negative control (untreated cells); Lanes 1-3: CSP-treated cells at 50, 100, and 200 µg/mL, respectively; Lanes 4-6: CSP-NiO-treated cells at 50, 100, and 200 µg/mL, showing enhanced DNA disruption compared to the control. The ncropped blot images are available in the Supplementary Figure S1.

## 4. Discussion

The emergence of green-synthesized metal oxide nanoparticles has attracted significant academic attention due to their environmentally friendly, cost-effective, and sustainable production routes that avoid the use of hazardous chemicals [38, 39]. Traditional chemical and physical synthesis routes often use toxic precursors, thus potentially compromising biocompatibility [40]. Therefore, the development of biologically mediated synthesis strategies is increasingly viewed as essential for improving the translational potential of metal oxide nanomaterials in therapeutic applications. Therefore, the development of bio-mediated synthesis methods is increasingly viewed as a key to improving the translational capabilities of metal-oxide nanomaterials in therapeutics [41, 42]. Recent studies have shown that nanoparticles, owing to their small size and increased surface reactivity, exhibit enhanced antimicrobial activity against a wide range of infectious microorganisms [43]. NiO NPs with high chemical stability and redox reactivity have attracted significant interest in numerous biomedical applications, including antitumor and antimicrobial capabilities [43, 44]. The present study addresses this challenge by utilizing CSP as a natural reducing and stabilizing agent for the green synthesis of NiO NPs. Polysaccharides, with their abundant hydroxyl groups, play a critical role in stabilizing metal ions during nanoparticle synthesis, as supported by previous studies [45-47]. NiO NPs have been reported to exert antibacterial effects through mechanisms involving ROS generation, metal ions release, and membrane destabilization in both Gram-positive and Gram-negative bacteria [48]. However, the relative contribution of these pathways is known to depend on nanoparticle synthesis route and surface chemistry, necessitating system-specific mechanistic evaluation. In this study, we explored the mechanism underlying the antimicrobial activity of CSP-NiO NPs against Gram-positive (*S. aureus* and *C. tetani*) and Gram-negative (*E coli* and *K. pneumoniae*) bacteria using different antimicrobial assays.

The successful formation of CSP-NiO NPs was confirmed by UV-visible spectroscopy, FTIR, SEM, XRD, and EDX, which revealed structural integrity and phase purity. The UV-visible absorbance peak at 350 nm and the characteristic Ni-O vibrations at ~570 cm$^{-1}$ were consistent with previously reported green-synthesized NiO NPs [49-51]. XRD patterns confirmed the cubic crystalline phase with diffraction peaks matching the standard NiO planes and a crystalline size of approximately 16.57 nm, further confirming the successful formation of NPs [52]. SEM analysis revealed agglomerated nanostructures, a common feature of green-synthesized metal oxide nanoparticles arising from hydrogen bonds and interparticle interactions. EDX analysis confirmed the elemental composition of nanoparticles, with Ni and O as the predominant elements. Minor carbon and trace element signals were also detected and are likely associated with residual polysaccharides, precursor salts, or sample preparation. However, their low relative abundance is unlikely to significantly influence the antibacterial effect of CSP-NiO NPs [53]. High-resolution Transmission Electron Microscopy (TEM) analysis would further clarify primary particle morphology and dispersion at the nanoscale.

Biocompatibility assessment demonstrated low hemolytic activity at the tested concentrations, consistent with prior reports of green-synthesized NiO NPs exhibiting acceptable hemocompatibility profiles. These findings suggest that polysaccharide-mediated surface stabilization may help maintain erythrocyte compatibility while preserving antibacterial function. The agar well diffusion assay demonstrated that CSP-NiO NPs inhibited bacterial growth in a dose-dependent manner. This enhanced activity is consistent with previously reported green NiO NPs, in which nanoparticle formation amplifies antimicrobial activity through increased surface-mediated oxidative interactions [54-56]. Because nanoparticle suspensions exhibit different diffusion behavior from standard antibiotic discs within agar matrices, inhibition zone measurements should be interpreted qualitatively [57, 58]. Therefore, agar well diffusion assay was complemented with MIC, MBC, and growth kinetic analyses to provide a more quantitative evaluation of antibacterial efficacy.

Greater susceptibility of Gram-positive strains relative to Gram-negative strains is consistent with structural differences in cell wall architecture. The thick peptidoglycan layer of Gram-positive bacteria may facilitate interaction with ROS. In contrast, the outer lipid membrane of Gram-negative bacteria acts as a permeability barrier limiting nanoparticle and ROS penetration [59, 60]. Similar susceptibility trends have been reported for other green-synthesized NiO and CuO nanoparticles, where surface charge and particle characteristics influence bacterial interaction dynamics [61]. Further incorporation of zeta potential analysis would enable the quantitative evaluation of electrostatic interactions between CSP-NiO NPs and bacterial cell surfaces.

Additionally, Brunauer-Emmett-Teller (BET) surface area analysis would clarify the role of surface properties in antibacterial activity. Growth kinetics supported the inhibitory effect of CSP-NiO NPs, demonstrating concentration-dependent suppression of bacterial proliferation. This current inhibition pattern aligns with previously reported findings on NiO nanoparticles synthesized using *Aloe vera* and *Ocimum sanctum*, in which oxidative stress and ion-mediated interactions collectively impair metabolic progression and cell division [62, 63].

Mechanistically, CSP-NiO NPs induced elevated intracellular ROS levels, membrane protein leakage, and genomic DNA fragmentation. These observations are consistent with the established oxidative stress-mediated antibacterial mechanism of NiO nanoparticles, in which ROS generation disrupts membrane integrity and promotes macromolecular damage [64, 65]. DNA fragmentation further supports the notion that oxidative genotoxic stress as a downstream consequence of membrane destabilization and cellular redox imbalance. Similar DNA degradation has been reported for NiO and ZnO nanoparticles in *E.coli*, suggesting that ROS-mediated damage and possible electrostatic interactions between $Ni^{2+}$ ions and bacterial DNA may contribute to nanoparticle-induced antibacterial activity [66].

The qualitative DNA fragmentation patterns observed in the present study further support oxidative genotoxic damage; however, quantitative densitometric analysis would provide greater resolution in assessing the extent of DNA damage. Complementary oxidative stress markers, including lipid peroxidation and antioxidant enzyme assays, would further strengthen mechanistic validation. In addition, direct quantification of $Ni^{2+}$ ion release and membrane potential disruption assays was not conducted; therefore, the relative contribution of ion-mediated mechanisms remains inferential and warrants further investigation. Protein leakage was not normalized to post-treatment biomass, and future studies may incorporate this normalization to improve quantitative precision.

## Conclusion

The present study demonstrates the facile, biologically mediated synthesis of NiO NPs utilizing polysaccharides derived from *Lepidium sativum* seeds, confirming their crystalline structure and surface stabilization. This green synthesis produced CSP-NiO NPs exhibiting dose-dependent antibacterial activity and low hemolytic effects under the tested in vitro conditions. Mechanistic investigations indicated that the bactericidal activity is primarily mediated by ROS-induced oxidative stress, leading to membrane damage, protein leakage, and genomic DNA damage, with Gram-positive strains showing greater susceptibility. These findings highlight the potential of CSP as a sustainable biomatrix for nanoparticle synthesis and support the antibacterial efficacy of CSP-NiO NPs. However, further studies evaluating long-term nanoparticle stability, in vivo toxicity, pharmacokinetics, and environmental impact are necessary before considering translational or clinical applications.

## Declarations

**Competing interests:** The authors declare that they have no conflict of interest.

**Ethics approval and consent to participate:** This article does not contain any studies with human participants or animals performed by any of the authors.

**Data availability:** The datasets used and analyzed during the current study are available from the corresponding author on reasonable request.

**Authors' contributions:** Y.J., M.A., S.A., A.A: methodology, data collection, original data analysis, writing original draft; A.A: supervision, A.A., and S.A: data presentation, writing and editing of manuscript; D.L: data collection, software; A.F.A, S.A., and A.A: validation, software, visualization, resources, writing original draft, funding acquisition, and revision of the manuscript. All authors have read and agreed to the published version of the manuscript.

**Consent for publication:** All the authors have approved the paper for publication.

**Funding:** This research work was supported by the Higher Education Department, Government of Khyber Pakhtunkhwa, under the Higher Education Research Endowment Fund (HEREF), Project No. 3111, and the Higher Education Commission of Pakistan, Project No. NRPU-10569.

**Acknowledgments:** We are very thankful to the Ongoing Research Funding program (ORF-2025-218) at King Saud University, Riyadh, Saudi Arabia.

## References

1. Puri, B., R. Vaishya, and A. Vaish, *Antimicrobial resistance: Current challenges and future directions.* Medical Journal Armed Forces India 2025. **81**(3): p. 247-258.
2. Nazir, A., et al., *The global challenge of antimicrobial resistance: mechanisms, case studies, and mitigation approaches.* Health Science Reports 2025. **8**(7): p. e71077.
3. Auzin, A., et al., *What is the evidence base of used aggregated antibiotic resistance percentages to change empirical antibiotic treatment? A scoping review.* Clinical Microbiology 2022. **28**(7): p. 928-935.
4. Tarin-Pello, A., B. Suay-Garcia, and M.-T. Perez-Gracia, *Antibiotic resistant bacteria: current situation and treatment options to accelerate the development of a new antimicrobial arsenal.* Expert review of anti-infective therapy 2022. **20**(8): p. 1095-1108.
5. Sharmin, S., et al., *Nanoparticles as antimicrobial and antiviral agents: A literature-based perspective study.* Heliyon 2021. **7**(3).
6. Tijani, N.A., et al., *Metallic nanoparticles: a promising novel therapeutic tool against antimicrobial resistance and spread of superbugs.* BioMetals 2025. **38**(1): p. 55-88.

7. Do, H.T.T., et al., *Advances in silver nanoparticles: unraveling biological activities, mechanisms of action, and toxicity.* Applied Nanoscience 2025. **15**(1): p. 1.

8. Rani, L. and R. Chauhan, *Transition metal (Mn-, Ni-, Co-and Cu-) doped ZnS nano-flowers for morphological, structural, optical, elemental and antibacterial studies.* Transition Metal Chemistry 2025: p. 1-20.

9. Ramesh, S., et al., *Fabrication of cobalt oxide@ cellulose/nitrogen doped carbon nanotubes decorated metal organic frameworks composite for symmetric supercapacitor applications.* Journal of Power Sources 2025. **631**: p. 236288.

10. Brown, C.D., et al., *Synthesis and characterization of PVP-coated tellurium nanorods and their antibacterial and anticancer properties.* Journal of Nanoparticle Research 2018. **20**(9): p. 254.

11. Khan, A., et al., *Green Synthesis of Metal-Oxide Nanoparticles from Fruits and Their Waste Materials for Diverse Applications*, in *Nanomaterials from Agricultural and Horticultural Products*. 2023, Springer. p. 81-119.

12. Jaji, N.-D., et al., *Advanced nickel nanoparticles technology: From synthesis to applications.* Nanotechnology reviews 2020. **9**(1): p. 1456-1480.

13. Iqbal, S., et al., *Toxicity assessment of metallic nickel nanoparticles in various biological models: An interplay of reactive oxygen species, oxidative stress, and apoptosis.* Toxicology Industrial Health 2021. **37**(10): p. 635-651.

14. Huynh, K.G., et al., *Surface Modifications of Zinc Oxide, Copper Oxide, and Nickel Oxide Particles with Chitosan, Poly (ethylene glycol), Poly (vinyl alcohol), and Poly (vinylpyrrolidone) as Antimicrobial Agents against Staphylococcus aureus, Pseudomonas aeruginosa, and Salmonella enterica.* ACS omega 2025. **10**(43): p. 51962-51984.

15. Behera, N., et al., *Oxidative stress generated at nickel oxide nanoparticle interface results in bacterial membrane damage leading to cell death.* RSC advances 2019. **9**(43): p. 24888-24894.

16. Terreni, M., M. Taccani, and M. Pregnolato, *New antibiotics for multidrug-resistant bacterial strains: latest research developments and future perspectives.* Molecules 2021. **26**(9): p. 2671.

17. Kumar, J.A., et al., *A focus to green synthesis of metal/metal based oxide nanoparticles: Various mechanisms and applications towards ecological approach.* Journal of Cleaner Production 2021. **324**: p. 129198.

18. Seth, R. and A. Meena, *Enzymes-based nanomaterial synthesis: an eco-friendly and green synthesis approach.* Clean Technologies Environmental Policy 2025. **27**(10): p. 5775-5798.

19. Khan, S.A., et al., *Phytomolecules-coated NiO nanoparticles synthesis using abutilon indicum leaf extract: antioxidant, antibacterial, and anticancer activities.* International Journal of Nanomedicine 2021: p. 1757-1773.

20. Plucinski, A., Z. Lyu, and B.V. Schmidt, *Polysaccharide nanoparticles: from fabrication to applications.* Journal of Materials Chemistry B 2021. **9**(35): p. 7030-7062.

21. Liu, J., S. Willför, and C. Xu, *A review of bioactive plant polysaccharides: Biological activities, functionalization, and biomedical applications.* Bioactive carbohydrates dietary fibre 2015. **5**(1): p. 31-61.

22. Sidhu, A.K., N. Verma, and P. Kaushal, *Role of biogenic capping agents in the synthesis of metallic nanoparticles and evaluation of their therapeutic potential.* Frontiers in Nanotechnology, 2022. **3**: p. 801620.

23. Gupta, S. and R. Gupta, *Research update on the therapeutic potential of garden cress (Lepidium sativum Linn.) with threatened status.* Current Drug Research Reviews Formerly: Current Drug Abuse Reviews 2024. **16**(3): p. 369-380.

24. Shiam, M.A.H., et al., *A review of plant-derived gums and mucilages: Structural chemistry, film forming properties and application.* Journal of Plastic Film Sheeting 2025. **41**(2): p. 195-237.

25. Khan, I.U., et al., *Pichia pastoris Mediated Digestion of Water-Soluble Polysaccharides from Cress Seed Mucilage Produces Potent Antidiabetic Oligosaccharides.* Pharmaceuticals 2024. **17**(6): p. 704.

26. Khan, I.U., et al., *Anti-oxidative and anti-apoptotic oligosaccharides from pichia pastoris-fermented cress polysaccharides ameliorate chromium-induced liver toxicity.* Pharmaceuticals 2024. **17**(7): p. 958.

27. Khan, I.U., et al., *Unlocking the in vitro and in vivo antioxidant and anti-inflammatory activities of polysaccharide fractions from Lepidium sativum seed-coat mucilage.* Heliyon 2024. **10**(17).

28. Shiehnezhad, M., S. Zarringhalami, and N. Malekjani, *Optimization of Microwave-Assisted Extraction of Mucilage from Ocimum basilicum var. album (L.) Seed.* Journal of Food Processing Preservation 2023. **2023**(1): p. 5524621.

29. Xiaolong, J., et al., *Research progress on degradation methods and product properties of plant polysaccharides.* Journal of Light Industry 2023. **38**(3).

30. Mirsalari, F., E. Tahanpesar, and H. Sanaeishoar, *Biosynthesis of NiO-NPs using mucilage of Cordia myxa fruit and their potential application as an efficient catalyst for the synthesis of chromenes.* Research on Chemical Intermediates 2023. **49**(9): p. 4127-4148.

31. Singh, A., et al., *Structurally and morphologically engineered single-pot biogenic synthesis of NiO nanoparticles with enhanced photocatalytic and antimicrobial activities.* Journal of Cleaner Production 2022. **343**: p. 131026.

32. Güler, Ş., et al., *Evaluation of antibacterial efficacy of Lawsonia inermis Linn (henna) on periodontal pathogens using agar well diffusion and broth microdilution methods: an in-vitro study.* BioMedicine 2023. **13**(3): p. 25.

33. Rahman, A., et al., *Facile Synthesis and Application of Ag-NPs for Controlling Antibiotic-ResistantPseudomonas spp. and Bacillus spp. in a Poultry Farm Environment.* Journal of Nanotechnology 2023. **2023**(1): p. 6260066.

34. Sondi, I. and B. Salopek-Sondi, *Silver nanoparticles as antimicrobial agent: a case study on E. coli as a model for Gram-negative bacteria.* Journal of colloid interface science 2004. **275**(1): p. 177-182.

35. Ogami, A., et al., *Pathological features of different sizes of nickel oxide following intratracheal instillation in rats.* Inhalation toxicology 2009. **21**(10): p. 812-818.

36. Sahoo, B., et al., *Oxidative stress generated due to photocatalytic activity of biosynthesized selenium nanoparticles triggers cytoplasmic leakage leading to bacterial cell death.* RSC advances 2023. **13**(17): p. 11406-11414.

37. Yılmaz, H., et al., *DNA fragmentation, chromosomal aberrations, and multi-toxic effects induced by nickel and the modulation of Ni-induced damage by pomegranate seed extract in Allium cepa L.* Environmental Science Pollution Research 2023. **30**(51): p. 110826-110840.

38. Radulescu, D.-M., et al., *Green synthesis of metal and metal oxide nanoparticles: a review of the principles and biomedical applications.* International Journal of Molecular Sciences 2023. **24**(20): p. 15397.

39. Guo, M., et al., *Characterization and binding site profiling of zinc-chelated peptides from Takifugu rubripes bone with enhanced biological activity.* Food chemistry, 2025: p. 146627.

40. Kirubakaran, D., et al., *A comprehensive review on the green synthesis of nanoparticles: advancements in biomedical and environmental applications.* Biomedical Materials Devices 2026. **4**(1): p. 388-413.

41. Negrescu, A.M., et al., *Metal oxide nanoparticles: review of synthesis, characterization and biological effects.* Journal of Functional Biomaterials 2022. **13**(4): p. 274.

42. Malik, S., K. Muhammad, and Y. Waheed, *Emerging applications of nanotechnology in healthcare and medicine.* Molecules 2023. **28**(18): p. 6624.

43. Skłodowski, K., et al., *Metallic nanosystems in the development of antimicrobial strategies with high antimicrobial activity and high biocompatibility.* International journal of molecular sciences 2023. **24**(3): p. 2104.

44. Talib, W.H., et al., *Natural Products and Altered Metabolism in Cancer: Therapeutic Targets and Mechanisms of Action.* International Journal of Molecular Sciences, 2024. **25**(17): p. 9593.

45. Bilal, M., et al., *Polysaccharides-based bio-nanostructures and their potential food applications.* International Journal of Biological Macromolecules 2021. **176**: p. 540-557.

46. Maind, R., et al., *Nickel Oxide Based Nanoparticles: Green Synthesis, Morphological Assessment, and Their Biological Properties.* Universal Journal of Green Chemistry 2024: p. 229-254.

47. Su, M., et al., *Astragalus improves intestinal barrier function and immunity by acting on intestinal microbiota to treat T2DM: a research review.* Frontiers in immunology, 2023. **14**: p. 1243834.

48. Behera, N., et al., *Oxidative stress generated at nickel oxide nanoparticle interface results in bacterial membrane damage leading to cell death.* RSC advances 2019. **9**(43): p. 24888-24894.

49. Iqbal, J., et al., *Green synthesis and characterizations of Nickel oxide nanoparticles using leaf extract of Rhamnus virgata and their potential biological applications.* Applied Organometallic Chemistry 2019. **33**(8): p. e4950.

50. Al-Zaqri, N., et al., *Green synthesis of nickel oxide nanoparticles and its photocatalytic degradation and antibacterial activity.* Journal of Materials Science: Materials in Electronics 2022. **33**(15): p. 11864-11880.

51. Wang, J., et al., *SIRT6 protects against lipopolysaccharide-induced inflammation in human pulmonary lung microvascular endothelial cells.* Inflammation, 2024. **47**(1): p. 323-332.

52. Haider, A.J., et al., *Photocatalytic activity of nickel oxide.* Journal of Materials Research Technology 2019. **8**(3): p. 2802-2808.

53. Hafeez, M., et al., *Green synthesis of nickel oxide nanoparticles using populus ciliata leaves extract and their potential antibacterial applications.* South African Journal of Chemistry 2021. **75**: p. 168–173-168–173.

54. Uddin, S., et al., *Green synthesis of nickel oxide nanoparticles using leaf extract of Berberis balochistanica: Characterization, and diverse biological applications.* Microscopy Research Technique 2021. **84**(9): p. 2004-2016.

55. Zhang, L., et al., *Ten-gram-scale mechanochemical synthesis of ternary lanthanum coordination polymers for antibacterial and antitumor activities.* Frontiers in Chemistry 2022. **10**: p. 898324.

56. Hassan, F., et al., *Potential of dietary hemp and cannabinoids to modulate immune response to enhance health and performance in animals: opportunities and challenges. Front Immunol 14: 1285052*. 2023.

57. Zhang, X., et al., *Analytical methods for assessing antimicrobial activity of nanomaterials in complex media: advances, challenges, and perspectives.* Journal of nanobiotechnology 2023. **21**(1): p. 97.

58. Chung, E., et al., *Applied methods to assess the antimicrobial activity of metallic-based nanoparticles.* Bioengineering 2023. **10**(11): p. 1259.

59. Berhe, M.G. and Y.T. Gebreslassie, *Biomedical applications of biosynthesized nickel oxide nanoparticles.* International journal of nanomedicine 2023: p. 4229-4251.

60. Yin, X., et al., *Multiple bacteria recognition mechanisms and their applications.* Coordination Chemistry Reviews 2024. **517**: p. 216025.

61. preet Singh, G., et al., *Green synthesis of NiO doped CuO nanoparticles: Potential for environmental remediation.* Inorganic Chemistry Communications 2023. **157**: p. 111250.

62. Ahmad, B., et al., *Green synthesis of NiO nanoparticles using Aloe vera gel extract and evaluation of antimicrobial activity.* Materials Chemistry Physics 2022. **288**: p. 126363.

63. Patil, O.P., et al., *Green Synthesis and Characterization of Zinc Oxide Nanoparticles Derived from Ocimum Sanctum Leaves: Antibacterial, Antibiofilm, and Thermal Studies.* Journal of Bio-and Tribo-Corrosion 2026. **12**(1): p. 34.

64. Cao, J., et al., *Mechanistic insight on nanomaterial-induced reactive oxygen species formation.* Journal of Environmental Sciences 2025. **151**: p. 200-210.

65. Modi, S.K., et al., *Mechanistic insights into nanoparticle surface-bacterial membrane interactions in overcoming antibiotic resistance.* Frontiers in microbiology 2023. **14**: p. 1135579.

66. Aslinjensipriya, A., et al., *Revealing the Substitution of Zn2+ on Nano-Structural, Magneto-Electrical, Antibacterial and Antifungal Attributes of Nickel Oxide Nanoparticles via Sol-Gel Strategy.* 2022.